LIQUID CRYSTALS, 1987, VOL. 2, NO. 3, 313–334

Computer simulation studies of anisotropic systems XVI. The smectic E–smectic B transition

by G. R. LUCKHURST and P. SIMPSON†
Department of Chemistry, The University, Southampton SO9 5NH, England
and C. ZANNONI
Istituto di Chimica Fisica, Universitá di Bologna, 40136 - Bologna, Italy

(*Received 25 September 1986; accepted 19 January 1987*)

We have investigated the smectic E–smectic B transition with the aid of a model smectogen whose properties have been calculated using the Monte Carlo technique of computer simulation. The lath-like mesogenic molecules are defined to lie in a plane with their centres on a triangular lattice and with their long axes orthogonal to the smectic layer. The quadrupolar interaction, restricted to nearest neighbours, is assumed to be responsible for the herring-bone arrangement of the molecular short axes, characteristic of the smectic E phase. The computer simulations have been employed to evaluate both thermodynamic and structural parameters as a function of temperature. The model smectogen is found to exhibit a continuous transition at which the long range herring-bone structure of the smectic E phase is destroyed only to be replaced by the analogous short range structure of the smectic B. Where possible the results simulated for the model smectogen are compared with the behaviour of real mesogens and the predictions of molecular field theories for the transition. In particular, contact is made with X-ray diffraction studies of the two phases by using optical techniques to generate the diffraction patterns associated with configurations produced by the simulation. The model is found to be in good accord with experiment but the molecular field prediction of the smectic E–smectic B transition temperature is shown to be poor.

1. Introduction

It is frequently assumed that the molecules which constitute thermotropic liquid crystals are cylindrically symmetric about their long axes. In fact the molecules are more lath-like than rod-like because of the phenyl rings which are an integral part of most mesogenic molecules as, for example, in 4-phenylbenzylidene-4′-amino-*n*-pentyl cinnamate (I)

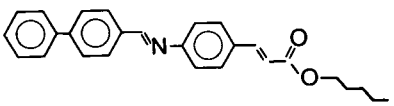

(I)

One intriguing consequence of this molecular biaxiality is that the uniaxial nematic phase should undergo a transition to a biaxial nematic at a lower temperature [1]. However it has not proved possible to cool a real nematic to sufficiently low temperatures to reveal the biaxial phase, although it has been observed for a model nematogen by a computer simulation experiment [2].

† Present address: Royal Signals and Radar Establishment, Great Malvern, Worcestershire WR14 3PS, England.

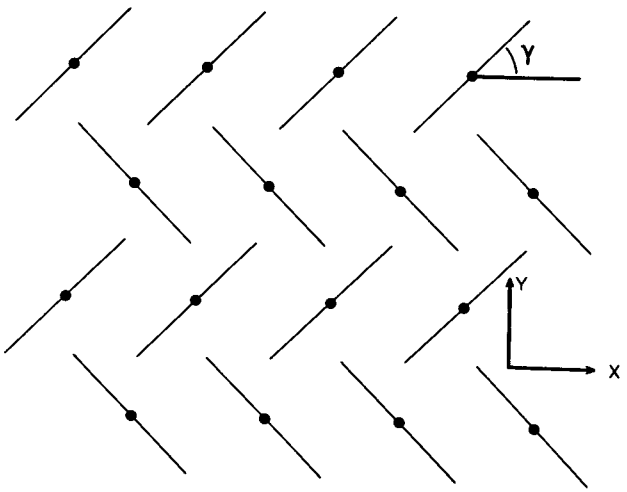

Figure 1. The classical herring-bone arrangement of the molecular short axes in a smectic E phase. The laboratory axes x and y, used to describe the molecular orientations, are taken to be parallel to the two glide planes of the herring-bone structure.

The situation is different for smectic phases where the influence of molecular biaxiality on the organization within the layers of certain smectic phases has been established [3]. For example within the smectic B phase the molecules are arranged on the sites of a hexagonal lattice with their long axes essentially orthogonal to the layers. There is no long range orientational correlation between the molecular short axes and so the phase is uniaxial. In the smectic E phase, however, such long range ordering is present and, on average, the short axes form a herring-bone structure (cf. figure 1); in consequence the phase is biaxial.

The structures of both the smectic B and E phases have been established by careful diffraction studies on a range of materials [4–7] which includes (I). In addition such investigations [4, 6] also reveal that within the smectic E phase the molecules are arranged on an orthorhombic lattice which results from a small distortion of the hexagonal structure of the smectic B phase. For mesogens possessing both phases the smectic E–smectic B transition is found to be weakly first order [8]. We are unaware of any experimental determination of the orientational order parameters characterizing the fluctuations of the molecular short axes with respect to their preferred orientation or director.

There have been several attempts to develop a theoretical description of the smectic E–smectic B transition. These share a common feature in that they consider a single smectic layer; such an approximation seems reasonable because although the molecular centres are correlated over many layers the orientations of the short axes do not appear to be well correlated between layers [7]. In the first theoretical analysis Meyer [9] discussed the possible contributions to the anisotropic intermolecular potential but then restricted the potential to that for quadrupolar forces when dealing with the smectic E–smectic B transition. This was treated within the molecular field approximation and the transition was predicted to be second order; the transition temperature was also related to the parameters occurring in the pair potential. In a subsequent paper [10] Meyer returned to the problem when he developed a Landau theory for the transition, which was again predicted to be second order. This prediction

conflicts with the weak first order transition which has been observed and so Meyer extended the theory to allow for the distortion of the lattice at the transition to the smectic E; with such an extension the theory is in accord with experiment. The influence of weak interactions between layers on the order of the transition was also considered although it was concluded that this would remain first order. The Landau theory of the smectic E–smectic B transition including lattice distortions has been redeveloped by Michelson and Cabib [11] using group theoretical arguments to describe the symmetry changes at the transition. They explore, in a natural way, the ground state structures given by the theory rather than use the known structures to construct the Landau expansion of the free energy density. They also predict the smectic E–smectic B transition to be second order even when the lattice distortions are included in the theory. In addition they criticize the work of Meyer [10] because, they claim, the ordering tensor employed in his theory is not sufficiently general and the coupling of the lattice distortion to the ordering tensor is strictly forbidden by the symmetry of the smectic phases. Later, the molecular field theory was redeveloped by Felsteiner *et al.* [12] starting from a pair potential of the same form as that for quadrupolar interactions. The theory was then used to explore the possible structures for the short axes for different choices of the parameters occurring in the pair potential. Only one of these structures, namely the herring-bone arrangement in the smectic E, has been observed. In addition the temperature for the smectic E–smectic B transition was also related to the parameters in the pair potential.

Here we adopt a different approach to investigate the smectic E–smectic B transition by using the Monte Carlo technique of computer simulation [13]. This has the merit of being able to calculate a wide range of properties for a model smectogen, in an essentially exact way. The nature of the model is described in the following section where we show how the quadrupolar intermolecular potential employed in the simulation is related to the general pair potential for rigid molecules of arbitrary shape. The Monte Carlo calculations are explained briefly in §3 where the various properties determined by the simulation are also described. These include thermodynamic properties as well as single particle orientational order parameters and various orientational correlation functions needed to characterize the structure of the phases. The results of the simulation are presented and discussed in the final section where we also predict the scattering patterns expected for the phases by using optical masking techniques [14].

The smectic E–smectic B transition has certain features in common with the rotational transition observed for molecular nitrogen adsorbed on graphite [15]. They differ primarily in that the internuclear vector of the nitrogen molecule, which is the equivalent of the short molecular axis of a smectogenic molecule, is not constrained to be parallel to the graphite surface [16] unlike the situation for the smectic phases. Attempts [17–19] have been made to understand the nature of this transition by using computer simulation techniques with models analogous to that which we have adopted [20]. However in our investigations we have concentrated on those features of the smectic E–smectic B transition which will be of prime interest to those concerned with these smectic phases. Indeed we trust that the detailed description of the transition exhibited by our model smectogen available from the simulation will stimulate more studies, both theoretical and experimental.

2. The intermolecular potential

The mesogens which exhibit a smectic E–smectic B transition are composed of non-rigid molecules but in developing a model to study with the aid of computer

simulations it is assumed that the particles are rigid. The pair potential for molecules of arbitrary shape may be expanded, quite generally, as

$$U_{ij} = \sum u^{kk'}_{LL'J}(r_{ij})\, S^{kk'}_{LL'J}(\Omega), \tag{1}$$

where r_{ij} is the intermolecular separation and Ω denotes, collectively, the orientations of the molecular axis systems (Ω_i, Ω_j) and the intermolecular vector ($\theta\phi$) in a laboratory frame [21]. The S-functions are defined by

$$S^{kk'}_{LL'J}(\Omega) = (i)^{L-L'-J} \sum \begin{pmatrix} LL'J \\ mm'M \end{pmatrix} D^{L}_{m,k}(\Omega_i) D^{L'}_{m',k'}(\Omega_j) C_{J,M}(\theta\phi), \tag{2}$$

where $\begin{pmatrix} LL'J \\ mm'M \end{pmatrix}$ is a Wigner $3j$ symbol, $D^{L}_{m,k}(\Omega_i)$ is a Wigner rotation matrix and $C_{J,M}(\theta\phi)$ is a modified spherical harmonic. X-ray diffraction studies suggest that the orientational order of the molecular long axis is high [7] and so we take the molecular z axis to be parallel to that of the laboratory frame, which is normal to the smectic layer. In addition such studies also show the orientational correlations between molecules in different layers to be weak; we shall therefore restrict our attention to a single molecular layer for which the intermolecular vector is orthogonal to the laboratory z axis. With these realistic assumptions the S-functions are reduced to

$$S^{kk'}_{LL'J}(\Omega) = (i)^{L-L'-J} \sum \begin{pmatrix} LL'J \\ kk'k + k' \end{pmatrix} \exp(ik\gamma_i) \exp(ik'\gamma_j)\, C_{J,k+k'}(\pi/2\,\phi), \tag{3}$$

where γ is the angle made by the molecular x axis with that of the laboratory frame. The molecular polarity does not seem to affect the smectic E–smectic B transition and so we take the molecules to possess a mirror plane orthogonal to the molecular z axis; this restricts L, L', k and k' to even values. Even with these assumptions the number of unknowns in the pair potential is impossibly large and so we shall restrict L and L' to a value of 2, since these give the first non-trivial terms in the expansion of the pair potential. The angular dependence of the pair potential then takes the form

$$\begin{aligned} U_{ij} = {} & a\cos 2(\gamma_i - \gamma_j) + b\{\cos 2(\gamma_i - \phi_{ij}) + \cos 2(\gamma_j - \phi_{ij})\} \\ & + c\cos 2(\gamma_i + \gamma_j - 2\phi_{ij}), \end{aligned} \tag{4}$$

where the coefficients a, b and c are related to the expansion coefficients $u^{kk'}_{22J}(r_{ij})$. The molecules in a smectic B phase and, to a good approximation, in a smectic E phase are arranged on a triangular network and in consequence the term $b\{\cos 2(\gamma_i - \phi_{ij}) + \cos 2(\gamma_j - \phi_{ij})\}$ does not contribute to the total potential energy of the system. The effective pair potential is therefore reduced further to

$$U_{ij} = a\cos 2(\gamma_i - \gamma_j) + c\cos 2(\gamma_i + \gamma_j - 2\phi_{ij}). \tag{5}$$

To evaluate the relative magnitude of the two remaining coefficients we assume that the dominant contributions to the pair potential responsible for the smectic E–smectic B transition result from quadrupolar interactions. Such an assumption is in accord with the herring-bone structure of the smectic E phase, as has been discussed elsewhere [9–12]. The expansion coefficients for a multipolar expansion of the pair potential are given by

$$u^{kk'}_{LL'J}(r_{ij}) = (4\pi\varepsilon_0)^{-1} \sum (-)^{L+L'} \{(2L + 2L' + 1)!/(2L)!(2L')!\}^{1/2} r_{ij}^{-L-L'-1} Q_{Lk} Q_{L'k'}, \tag{6}$$

where J is constrained to equal $L + L'$ [21]. The multipolar tensors Q_{Lk} are given in a molecular frame and ε_0 is the permittivity of free space. Substitution of this expression for the $u^{kk'}_{LL'J}(r_{ij})$ into equation (1) and combination with equation (5) gives

the effective pair potential as

$$U_{ij} = (Q_{22}^2/4\pi\varepsilon_0 r_{ij}^5)\{\cos 2(\gamma_i - \gamma_j) + (35/3)\cos 2(\gamma_i + \gamma_j - 2\phi_{ij})\} \quad (7)$$

because our previous assumption of a mirror plane of symmetry orthogonal to the molecular z axis ensures the equality of the components Q_{22} and Q_{2-2} of the quadrupolar tensor. Finally we shall restrict the interactions to nearest neighbours in order to simplify the simulations and for these particles we write the effective pair potential as

$$U_{ij} = \varepsilon\{\cos 2(\gamma_i - \gamma_j) + (35/3)\cos 2(\gamma_i + \gamma_j - 2\phi_{ij})\}. \quad (8)$$

The form of this pair potential is sketched in figure 2 both as a contour plot and in three dimensions for two molecules with their intermolecular vector parallel to the laboratory x axis. The potential energy surface contains four minima each corresponding to one molecule parallel to the intermolecular vector while the other molecule is orthogonal to it. This demonstrates the clear dominance of the second term in the pair potential, for the first term is a maximum when the particles are parallel irrespective of their orientation to the intermolecular vector. For a collection of molecules with

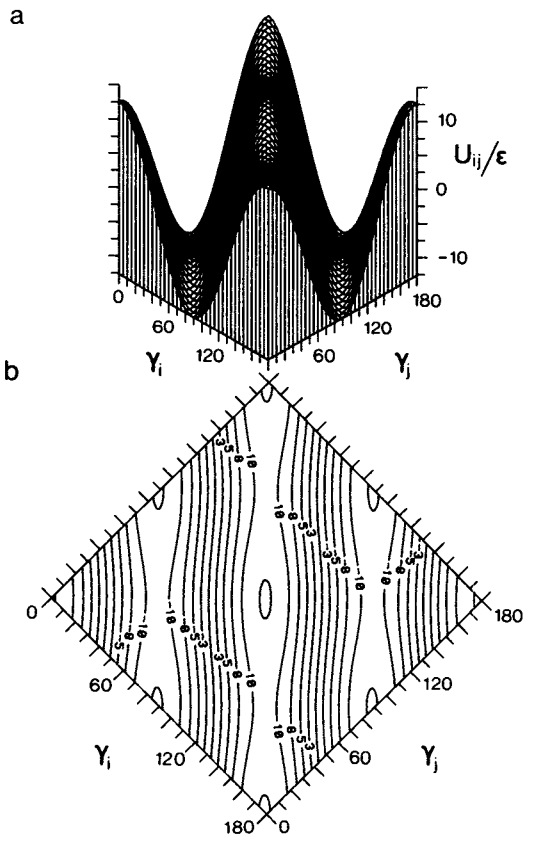

Figure 2. The effective pair potential (cf. equation (8)) employed in the simulations shown as a function of the molecular orientations in the laboratory frame with the intermolecular vector parallel to the x axis. The potential is given (*a*) in three dimensional and (*b*) in contour form.

their centres of mass restricted to the sites of a triangular lattice it is impossible to arrange all the molecular pairs so that they occupy these minima in the quadrupolar potential energy. We have therefore located the ground state of a system of 16 particles interacting via the nearest neighbour pair potential in equation (8) using a computational minimization procedure (NAG routine EO2CCF) to minimize the total potential energy with respect to the orientational coordinates; the ground state energy $\bar{U}/N\varepsilon$ is found to be $-24{\cdot}33$ where N is the number of particles. The ground state configuration is shown in figure 1; it is a perfect herring-bone structure as anticipated for quadrupolar interactions. The local structure of the six neighbours around a given molecule has two molecules parallel to the central particle and at 45° to the intermolecular vector while the remaining four are orthogonal to that at the centre and make angles of 15° and 135° with the intermolecular vector.

3. The Monte Carlo simulations

The system studied consisted of an array of 576 particles arranged on a triangular lattice. The simulation was performed using the standard procedures introduced by Metropolis *et al.* [22] with periodic boundary conditions. The orientation of the molecular x axis with respect to the laboratory frame was stored as γ and this was changed randomly according to

$$\gamma_{\text{new}} = \gamma_{\text{old}} + \Delta\{\zeta - (1/2)\}, \tag{9}$$

where ζ is a random number generated with a uniform distribution in the range 0 to 1 and Δ is the maximum displacement whose value is used to control the acceptance–rejection ratio. The particle whose orientation is to be changed was also selected at random. For each temperature, defined in terms of the scaled quantity $T^*(\equiv kT/\varepsilon)$, the total run consisted of an equilibration stage of about 1000 cycles where a cycle is N attempted moves. This was followed by a production run of between 4000 and 11 000 cycles, with the longer runs being used in the vicinity of the phase transition. The first temperature studied was T^* equal to 1·0 and for this the initial configuration was taken to be a perfect herring-bone with one of its glide planes parallel to the laboratory x axis (cf. figure 1). In principle any starting configuration could have been used; however the ground state structure is triply degenerate corresponding to the alignment of a glide plane along one of the three intermolecular vectors (i.e. corresponding to $\phi_{ij} = 0$, $\pi/3$ or $2\pi/3$). In consequence if the starting configuration had been totally disordered then on equilibration at a low temperature the herring-bone structure could have been formed in different parts of the system with a glide plane along different intermolecular vectors. An example of such a situation can be seen in figure 3 where two domains are present, one with the glide plane parallel to the x axis ($\phi_{ij} = 0$) and the other with ϕ_{ij} equal to $2\pi/3$. It has been predicted that such structures would require extensive equilibration runs before the system is annealed into a monodomain [23]. We decided therefore to start our series of calculations from a perfect herring-bone structure and to use the final configuration of the production run obtained from a lower temperature as the starting configuration for a simulation at a new temperature.

A variety of thermodynamic and structural properties were evaluated as a function of the scaled temperature. These included the scaled internal energy per particle $\bar{U}^*(\equiv \bar{U}/N\varepsilon)$ and the scaled heat capacity at constant volume per particle $C_v^*(\equiv \partial\bar{U}^*/\partial T^*)_v)$. This was obtained by numerical differentiation of the internal

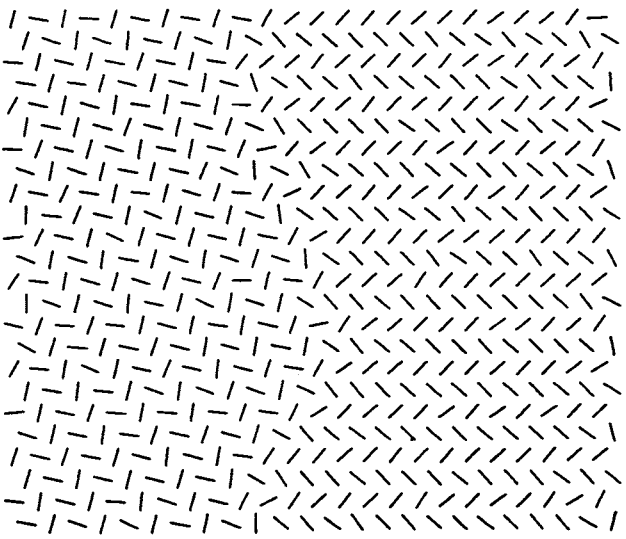

Figure 3. A configuration containing a domain wall separating two regions of the sample with their glide planes adopting different orientations in the laboratory frame. This was obtained at a scaled temperature of 1 from a simulation in which the starting configuration was totally disordered.

energy with respect to temperature using a cubic spline interpolation (CERN library routine E209). The heat capacity may also be obtained from the fluctuations in the internal energy [13]

$$C_v^* = (\overline{(U^{*2})} - \overline{U}^{*2})/T^{*2}, \tag{10}$$

but C_v^* is small for this system and the production runs employed in our simulations were not long enough to yield the heat capacity with sufficient accuracy.

The prime feature of the system is the destruction of the long range orientational order on passing from the smectic E to the smectic B mesophase and so we require a single particle order parameter with which to characterize this change. Such an order parameter must be defined as an average of some function of the angle made by the molecule with its preferred direction or director. In principle therefore we should need to locate the director during the course of the simulation experiment. Similar problems have been encountered in computer simulation studies of the nematic–isotropic transition and a variety of solutions have been proposed [13]. However, a glance at the herring-bone structure in figure 1 reveals that there is not a single director for the smectic E phase but two. This situation obtains because the structure is composed of molecules arranged on two sub-lattices each with their own director which are orthogonal to each other. In general the location of both directors would be a difficult task during the simulation and so we seek to define a long range orientational order parameter which is the same for both sub-lattices. For a two dimensional system the natural single particle orientational order parameters are the ensemble averages of the Chebychev polynomials, $\bar{T}_n(\equiv \overline{\cos n\gamma'})$ where γ' is the angle made by the molecular axis with the director. Such averages are the same for molecules on the two sub-lattices. However we only know the angle γ between the molecule and an arbitrary laboratory axis. We seek therefore to choose a value for the integer n such that the averages $\overline{\cos n\gamma^A}$ and $\overline{\cos n\gamma^B}$ for the sub-lattices A and B are identical. These averages

may be written in terms of the angles of α_A and α_B made by the two directors with respect to the laboratory axis; thus for the sub-lattice A

$$\begin{aligned}\overline{\cos n\gamma^A} &= \overline{\cos n(\gamma' - \alpha_A)} \\ &= \overline{\cos n\gamma'} \cos n\alpha_A, \end{aligned} \tag{11}$$

because the order parameters $\overline{\sin n\gamma'}$ vanish. There is a similar expression for $\overline{\cos n\gamma^B}$ which differs from that for sub-lattice A in the term $\cos n\,\alpha_B$ and so we need to select n such that

$$\cos n\alpha_A = \cos n\alpha_B. \tag{12}$$

The directors for the sub-lattices are orthogonal and so we require

$$\cos n\alpha_A = \cos(n\alpha_A - n\pi/2); \tag{13}$$

the lowest value of n satisfying this condition is 4. The averages $\overline{\cos 4\gamma}$ are therefore the same for the two sub-lattices. We now need to determine the director orientations α_A and hence α_B; this could be achieved by evaluating $\overline{\sin 4\gamma}$ and $\overline{\cos 4\gamma}$ since [24]

$$\tan 4\alpha_A = \tan 4\alpha_B = \overline{\sin 4\gamma}/\overline{\cos 4\gamma}. \tag{14}$$

Subsequently however we discovered that the glide plane for the herring-bone structure remained pinned along the laboratory x axis during all the simulations except perhaps close to the transition to the smectic B phase. This pinning is reminiscent of that observed for the director of the nematic phase formed by particles placed on a simple cubic lattice and interacting via anisotropic dispersion forces where again the pair potential depends on the orientation of the intermolecular vector [25]. Given the pinning of a glide plane in the smectic E phase we calculated three fourth rank order parameters namely $\overline{\cos 4(\gamma - \phi)}$ where ϕ, the orientation of the intermolecular vector, takes values 0, $\pi/3$ and $2\pi/3$; we denote them by $\bar{T}_4^0$, $\bar{T}_4^{\pi/3}$ and $\bar{T}_4^{2\pi/3}$. For the perfect herring-bone structure shown in figure 1 the order parameters take the values -1, $1/2$ and $1/2$ respectively and the same relationships exist between the three order parameters when the orientational order is incomplete. The order parameters were calculated by averaging over all the particles in the system at the end of every cycle in the production run. Since the two order parameters $\bar{T}_4^{\pi/3}$ and $\bar{T}_4^{2\pi/3}$ were indeed found to be equivalent in the simulations their average, which we denote by $\bar{T}_4^{\pi/3;2\pi/3}$, was determined.

As the transition to the smectic B phase is approached there is the possibility that the glide plane is no longer pinned along the lattice vector parallel to the x axis. In an attempt to check for such a change a fourth order parameter defined as the maximum value of the moduli of $\bar{T}_4^0$, $\bar{T}_4^{\pi/3}$ and $\bar{T}_4^{2\pi/3}$ was calculated; this is denoted by $\bar{T}_4^{\max}$.

To characterize the structural features of the phase in more detail, in particular the herring-bone structure of the smectic E phase, we have calculated several pair correlation functions; these monitor the distance dependence of the angular correlations [13, 26]. We have evaluated the total pair correlation functions of rank two and four; they are the analogues of the correlation functions encountered for three dimensional systems and are defined by

$$F_2(r_{ij}^*) = \overline{\cos 2\gamma_{ij}(r_{ij}^*)} \tag{15}$$

and

$$F_4(r_{ij}^*) = \overline{\cos 4\gamma_{ij}(r_{ij}^*)}. \tag{16}$$

Here r_{ij}^* is the scaled separation r_{ij}/a, where a is the lattice spacing, between particles i and j; γ_{ij} is the relative orientation $(\gamma_i - \gamma_j)$ of the two particles. In the large separation limit when the angular correlations are lost $F_4(r_{ij}^*)$ provides an alternative route to the fourth rank single particle order parameter $\bar{T}_4^0$, which we write as $\bar{T}_4$, for

$$\lim_{r_{ij}^* \to \infty} F_4(r_{ij}^*) = \bar{T}_4^2. \tag{17}$$

The situation is not quite so straightforward for $F_2(r_{ij}^*)$ because this does not vary smoothly with r_{ij}^* but adopts negative as well as positive values; this is apparent from a calculation of $F_2(r_{ij}^*)$ for the perfect herring-bone structure shown in figure 1. However the limiting value of the positive $F_2(r_{ij}^*)$ does yield the second rank single particle order parameter $\bar{T}_2$ which is defined as

$$\bar{T}_2 = \overline{\cos 2\gamma'}, \tag{18}$$

where γ' is the angle made by the molecular axis with the director. This situation obtains because for values of r_{ij}^* for which the second rank pair correlation function is positive the molecules are aligned with respect to the same director. The two correlation functions were determined at the end of every cycle for all pairs of particles with a scaled separation of 10 or less; this cut-off was imposed because of the excess correlations imposed by the periodic boundary conditions for larger separations [13]. At least 4000 configurations were used to calculate the correlation functions and these were taken from the end of the production run.

It is also of interest to monitor the orientational correlations along particular lattice vectors and so we have calculated the second rank anisotropic correlation functions

$$F_2(r_{ij}^*, \phi_{ij}) = \overline{\cos 2\gamma_{ij}(r_{ij}^*, \phi_{ij})}, \tag{19}$$

where ϕ_{ij} is the angle made by the lattice vector, containing particles i and j, with the laboratory x axis. We have, therefore, determined three anisotropic correlation functions with ϕ_{ij} equal to 0, $\pi/3$ and $2\pi/3$ which we denote by $F_2^0(r_{ij}^*)$, $F_2^{\pi/3}(r_{ij}^*)$ and $F_2^{2\pi/3}(r_{ij}^*)$, respectively. However, because a glide plane of the herring-bone structure is pinned along the x axis the correlation functions with ϕ_{ij} equal to $\pi/3$ and $2\pi/3$ should be equivalent. This proved to be the case and so $F_2^{\pi/3}(r_{ij}^*)$ and $F_2^{2\pi/3}(r_{ij}^*)$ were averaged. The correlation functions were calculated for the last configuration of each cycle and averaged over the entire production run.

4. Results and discussion

Here we describe the results obtained from our Monte Carlo simulation of the model mesogen and discuss them making contact, where possible, with experimental studies of the smectic E–smectic B transition. The numerical values of all the results, together with other details of the simulation described in this paper, have been deposited as a Supplementary Publication, comprising nine pages, with the British Library Document Supply Centre. Copies of these tables may be obtained by using the procedure described at the end of this issue and by quoting SUP 16503.

The scaled internal energy per particle is shown as a function of the scaled temperature over the wide range, 0 to 25, in figure 4. The internal energy is seen to increase continuously with temperature over the entire temperature range. However there appears to be a change in slope when T^* is in the vicinity of 10 and this change is revealed more clearly by the scaled heat capacity whose temperature dependence is

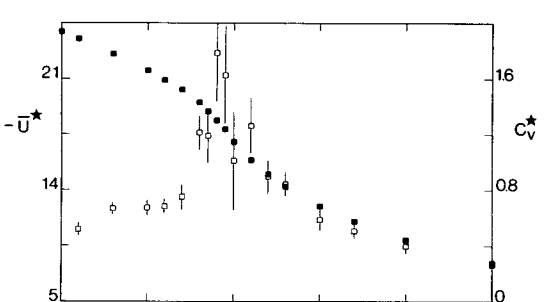

Figure 4. The dependence of the scaled internal energy per particle, $\bar{U}^*$ (■), and the scaled heat capacity per particle, C_v^* (□), on the scaled temperature, T^*.

also shown in figure 4. C_v^* is seen to exhibit a slight maximum when T^* is 9·3 ± 0·4; the error here largely reflects the separation in temperature of the simulations in this region. The unambiguous interpretation of a small peak in the heat capacity is difficult, especially for a simulation containing a modest number of particles. However, the maximum scaled heat capacity is only 1·7 which is small in comparison with the value of approximately 9 found for analogous lattice models of nematogens which exhibit weak, first order nematic–isotropic transitions [27]. Our results are then consistent with a higher order or continuous transition between the two phases and this is supported by the behaviour of other properties which we have calculated. The changes in the nature of the two phases are illustrated, in figure 5, by the single

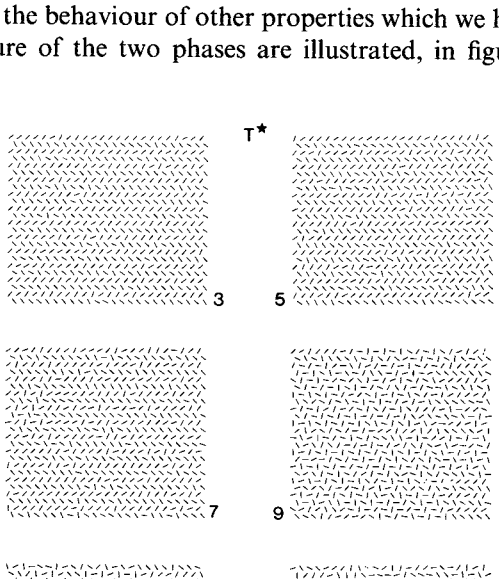

Figure 5. Configurations taken from the end of the production run for a selection of the temperatures at which the model mesogen was studied. The change in the molecular organization from a smectic E to a smectic B phase is clearly visible below and above T^* of 9.

configurations taken from the production stage for a selection of temperatures. At scaled temperatures below 9·4 the herring-bone structure, typical of the smectic E phase, is clearly apparent. One glide plane is found to be pinned along the x axis for T^* of 3, 5 and 7 but for the configuration shown for T^* equal to 9 the glide plane is no longer uniformly aligned along a particular lattice vector although for much of the sample it seems to be aligned at $2\pi/3$ to the x axis. At the higher scaled temperatures of 10 and 25 the long range herring-bone structure is destroyed and the phase has the random molecular orientations associated with a smectic B phase. In contrast to our model mesogen the smectic E–smectic B transition is found to be first order but with a small entropy of transition ($\Delta S/R \sim 0{\cdot}2$). However this first order character of the transition may well result from the distortion of the hexagonal lattice of the smectic B phase on forming the smectic E.

The simulation of the model smectogen is, however, consistent with the second order character of the phase transition predicted by the molecular field theories [9, 12]. None the less these theories fail to predict the smectic E–smectic B transition temperature with any accuracy, thus the scaled transition temperature is given by theory as 24·33 which yields the ratio of the predicted to observed transition temperatures as 2·59. This gross failure of the molecular field theories must result, in part, from the low dimensionality of the system for in three dimensions the molecular field approximation works well for the nematic–isotropic transition of the Lebwohl–Lasher nematogen where the ratio of predicted to observed transition temperatures is 1·18 [28]. However for a comparable system in two dimensions where the constituent particles interact via the $\cos 2(\gamma_i - \gamma_j)$ of the pair potential in equation (8) the ratio of the predicted to observed transition temperatures has increased significantly to 1·66 [24].

The simulation reported here is comparable to those used to investigate the structure of molecular nitrogen adsorbed on graphite. For example, Mouritsen and Berlinsky [18] simulated the behaviour of large numbers (up to 10^4) of particles located on a hexagonal lattice and interacting via the potential in equation (8) but without the $\cos 2(\gamma_i - \gamma_j)$ term. Their Monte Carlo simulation yielded a transition temperature which with our scaling parameter is 9·04. Although this is, within experimental error, equivalent to our result we should note that a later simulation by Evans *et al.* [19] in which the $\cos 2(\gamma_i - \gamma_j)$ is retained in the quadrupolar pair potential gives a transition temperature equal to $9{\cdot}39 \pm 0{\cdot}17$ which is identical to our result. We also note that for systems comparable in size to the one which we have studied Mouritsen and Berlinsky found the transition to be continuous, however when the number of particles was increased to 10^4 the transition was observed to be weakly first order [18]. These authors point out that the first order transition is in agreement with a renormalization group calculation on a system belonging to the same universality class as the quadrupolar system; that is the Heisenberg model with face type cubic anisotropy in two dimensions. Since these aspects are discussed in detail elsewhere [18] we shall not repeat them here.

We turn now to the structural parameters determined from the simulation and we begin with the fourth rank single particle order parameters $\bar{T}_4^0$, $\bar{T}_4^{\pi/3;2\pi/3}$ and $\bar{T}_4^{\max}$. These are shown as a function of the scaled temperature in figure 6. As expected the order parameters decrease in magnitude with increasing temperature but do not vanish exactly at the transition temperature of 9·3. In addition the order parameters vary continuously through the transition; such behaviour is to be anticipated from the continuous nature of the transition and the rounding of the transition which results from the relatively small number of particles employed in the simulation [29]. Except

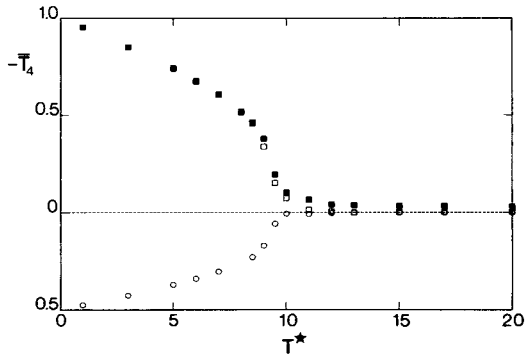

Figure 6. The temperature dependence of the fourth rank single particle orientational order parameters $\bar{T}_4^0$, $\bar{T}_4^{\pi/3;2\pi/3}$ and $\bar{T}_4^{\max}$; these are denoted by (■), (○) and (□), respectively.

in the close vicinity of the phase transition the values of $\bar{T}_4^0$ and $\bar{T}_4^{\max}$ are identical, which shows that one glide plane of the herring-bone structure is accurately pinned along the x axis.

The fourth rank order parameter $\bar{T}_4$ determined from the long range limit of the total fourth rank pair correlation function is shown as a function of the scaled temperature in figure 7. These results are found to be in good agreement with $\bar{T}_4^0$. The second rank order parameter $\bar{T}_2$ obtained from the long range limit of the positive values of $F_2(r_{ij}^*)$ are also plotted as a function of scaled temperature in figure 7. $\bar{T}_2$ is always greater than $\bar{T}_4$ and at low temperatures it decreases slowly with increasing T^* until at the transition $\bar{T}_2$ drops rapidly to essentially zero in the smectic B phase, indeed the change in $\bar{T}_2$ appears to be discontinuous. However $\bar{T}_2$ is expected to be greater than $\bar{T}_4$. This situation obtains because the orientational order parameters are given by the convolution

$$\bar{T}_n = \int_0^{2\pi} T_n(\cos\gamma')f(\gamma')\,d\gamma', \tag{20}$$

where $f(\gamma')$ is the singlet distribution function for the molecular orientation with respect to the director. Since the distribution is expected to be peaked at γ' equal to zero and $T_4(\cos\gamma')$ contains more nodes than $T_2(\cos\gamma')$ then the averages must satisfy the inequality $\bar{T}_2 \geqslant \bar{T}_4$. It may be this factor, combined with the sparcity of points near the transition, which produces the apparent discontinuous change in $\bar{T}_2$; in any event the continuous nature of the transition is indicated by the temperature dependence of the heat capacity.

The two order parameters can be used to explore the form of the singlet distribution function; this is related to the potential of mean torque, $U(\gamma')$, which a molecular experiences by

$$f(\gamma') = Z^{-1}\exp\{-U(\gamma')/kT\}, \tag{21}$$

where the orientational partition function

$$Z = \int_0^{2\pi} \exp\{-U(\gamma')/kT\}\,d\gamma' \tag{22}$$

provides the normalization. The potential may be expanded in a basis of Chebychev

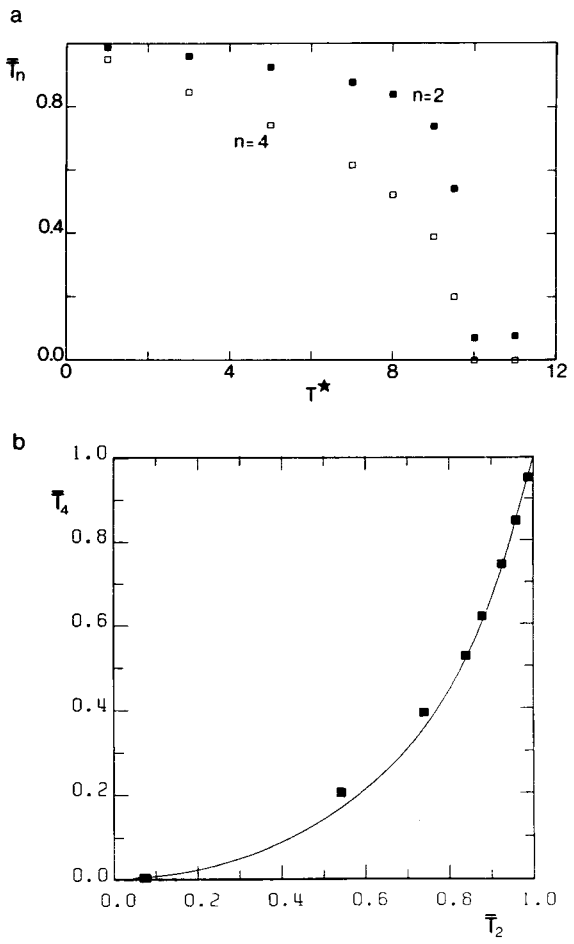

Figure 7. (*a*) The second (■) and fourth (□) rank single particle order parameters, $\bar{T}_2$ and $\bar{T}_4$ respectively, shown as a function of the scaled temperature, T^*. (*b*) The dependence of $\bar{T}_4$ on $\bar{T}_2$ obtained from the simulation (□) and predicted by the molecular field theory (——).

polynomials as

$$U(\gamma) = -\sum_{n(\text{even})} a_n T_n(\cos\gamma), \tag{23}$$

where the symmetry of the phase restricts the summation to even values of n. According to a molecular field analysis of the quadrupolar interaction the series may be truncated after the second rank term [9, 12]. In addition this truncated form of the potential is obtained via the principle of maximum entropy as that which yields the best singlet distribution function when only the second rank order parameter, $\bar{T}_2$, is known [30]. However we have determined $\bar{T}_4$ as well as $\bar{T}_2$ from the simulation and so we can use this additional information to test the proposed truncation of the potential of mean torque. We do this by using equations (20–23) to write the order parameters as

$$\bar{T}_n = I_{n/2}(a_2/kT)/I_0(a_2/kT), \tag{24}$$

where $I_n(x)$ denotes an nth order modified Bessel function and hence to calculate $\bar{T}_2$ and $\bar{T}_4$ as a function of a_2/kT. The results of these calculations are shown as the solid line in figure 7 (*b*) where $\bar{T}_4$ is plotted as a function of $\bar{T}_2$; the data obtained from the simulations are included in the same figure. The good agreement between the predicted and the simulated dependence of $\bar{T}_4$ on $\bar{T}_2$ supports the orientational dependence of the potential of mean torque given by the molecular field theory.

The total pair correlation function, from which $\bar{T}_2$ and $\bar{T}_4$ were determined, are shown in figure 8 as a function of the scaled separation for a selection of temperatures studied in the simulation. In the perfectly ordered herring-bone structure $F_4(r_{ij}^*)$ is independent of r_{ij}^* and equal to unity; this behaviour is exhibited clearly by the results at T^* of 1. As the temperature is increased so the extent of the orientational correlations decreases although it is of interest to note that within the smectic E phase $F_4(r_{ij}^*)$

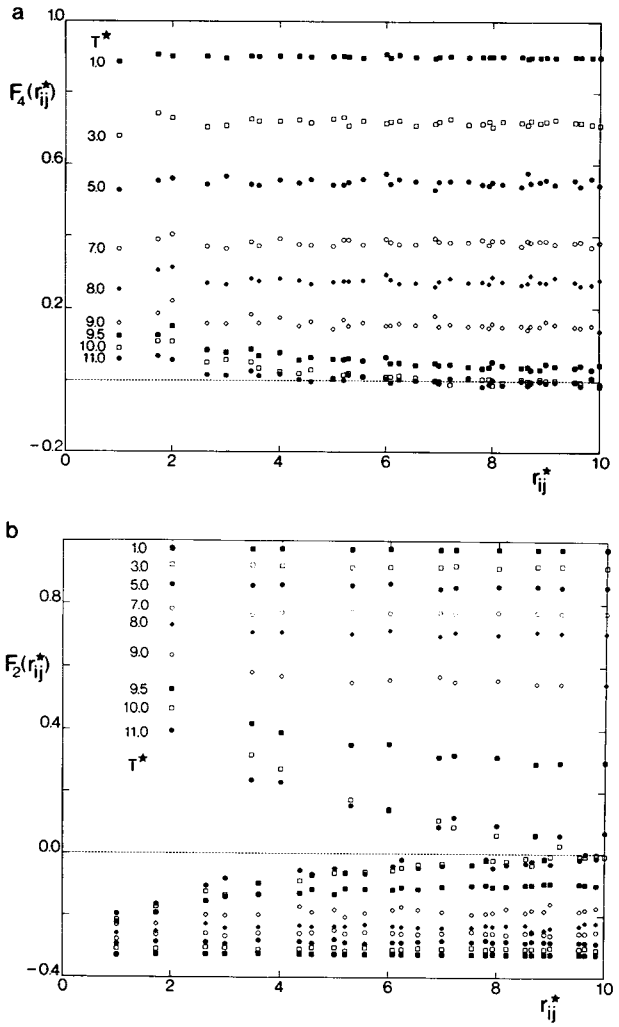

Figure 8. The dependence of the total orientational pair correlation functions on the scaled separation, r_{ij}^*, for a selection of the temperatures studied: (*a*) for the fourth rank function, $F_4(r_{ij}^*)$ and (*b*) for the second rank function, $F_2(r_{ij}^*)$.

reaches its limiting value at quite small separations r_{ij}^*, typically about 2, corresponding to the third shell of neighbours. It is also noticeable that the correlation function increases from its initial value with increasing separation before decreasing again to its long range limit. This feature is also apparent in the smectic B, for T^* greater than 9·5, but now the correlation function does not decay to its limiting value until the scaled separation is greater than about 5. We shall consider possible explanations for the slight maximum exhibited by $F_4(r_{ij}^*)$, shortly.

The total fourth rank correlation function is informative because it shows that the angular correlations are relatively insensitive to the molecular separation within the smectic E, at least until the vicinity of the transition is reached. However $F_4(r_{ij}^*)$ reveals nothing about the herring-bone structure of the smectic E phase. This is not the case for the total second rank correlation function which for a perfectly ordered herring-bone takes values 1 and $-1/3$ in a characteristic manner, for in some coordination shells all of the particles are parallel to that at the origin while for others only one third are parallel, the remaining two-thirds being orthogonal to the central particle. This particular variation is shown quite clearly by the results given in figure 8 (*b*) for a scaled temperature of 1. This variation in the sign of $F_2(r_{ij}^*)$, which serves as a fingerprint for the herring-bone structure, persists as the temperature is increased although the magnitude of the orientational correlations decreases. The positive and negative values of the second rank correlation function also decay rapidly with increasing separation to their non-zero values within the smectic E at least for temperatures less than 9·0, typically by a scaled separation of 3. However in the vicinity of the phase transition this decay length for the local orientational correlations begins to grow; here we use the term *decay length* instead of *correlation length* because in the smectic E phase orientational correlations persist in the long range limit. Just above the transition, in the smectic B phase at a scaled temperature of 10, $F_2(r_{ij}^*)$ has not decayed to its limiting value of zero until r_{ij}^* has reached its maximum value of 10. As the temperature is increased further the correlation length together with the local orientational correlations decrease further. The pretransitional growth in the decay length and the correlation length as the transition is approached is seen therefore to be symmetric about the transition. Finally we note that although the long range structural order of the smectic E phase is destroyed at the transition a local herring-bone structure is preserved, indeed this local structure has been inferred from the X-ray diffraction patterns observed for the smectic B [7].

A more informative view of the molecular organization within a monodomain of a smectic E phase is available from the anisotropic second rank correlation functions. $F_2(r_{ij}^*, \phi_{ij})$. The results for the two independent correlation functions, $F_2^0(r_{ij}^*)$ and $F_2^{\pi/3;2\pi/3}(r_{ij}^*)$, are shown in figure 9 for a selection of the scaled temperatures studied in the simulation. We see that within the smectic E phase $F_2^0(r_{ij}^*)$ decays rapidly to its long range limit whereas the average $F_2^{\pi/3;2\pi/3}(r_{ij}^*)$ oscillates between negative and positive values of essentially equal magnitude. The origin of this distinctive behaviour is readily understood by considering these functions for a perfect herring-bone structure with one glide plane parallel to the laboratory x axis (cf. figure 1). Along the glide plane, corresponding to the lattice vector with ϕ_{ij} equal to zero the particles are parallel to each other and so $F_2^0(r_{ij}^*)$ is equal to one and independent of the scaled separation. However along the other two lattice vectors ($\phi_{ij} = \pi/3$ and $2\pi/3$) for which $F_2(r_{ij}^*, \phi_{ij})$ were calculated the molecules are alternately orthogonal and parallel to that at the origin; in consequence $F_2^{\pi/3;2\pi/3}(r_{ij}^*)$ alternates between -1 and 1. The characteristic forms of the anisotropic correlation functions are clearly discernible at

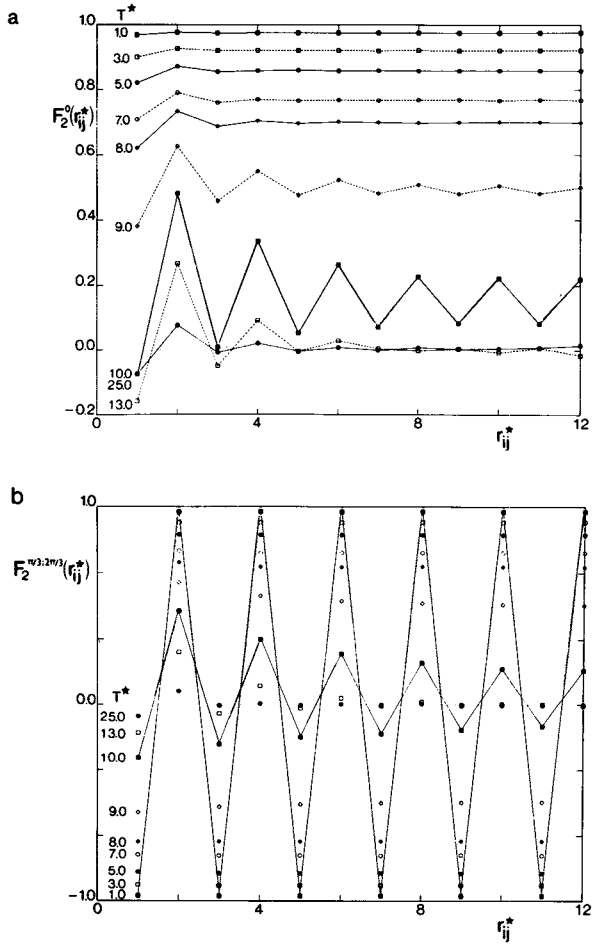

Figure 9. The dependence of the anisotropic second rank orientational correlation functions on the scaled separation, r_{ij}^*, for a selection of the scaled temperatures, T^*, studied in the simulation: (*a*) $F_2^0(r_{ij}^*)$ and (*b*) $F_2^{\pi/3;2\pi/3}(r_{ij}^*)$.

the lowest scaled temperature of 1 (cf. figure 9) in accord with the herring-bone structure (cf. figure 1). As the temperature is increased within the smectic E phase so the extent of the orientational correlations decreases, as we can see from figures 9 (*a*) and (*b*). In addition the short range order, with its slight maximum at r_{ij}^* of 2, is apparent prior to the correlation functions attaining their long range limits beyond a scaled separation of about 4. At a reduced temperature of 9, just before the phase transition, $F_2^0(r_{ij}^*)$ exhibits an alternation which becomes more marked at T^* of 10 although now the long range limit is considerably reduced. At still higher temperatures within the smectic B these oscillations are considerably diminished and the correlation function decays rapidly to its long range limit of zero. The alternation in $F_2^0(r_{ij}^*)$ obtains because in the vicinity of the transition, regions of the sample develop where the glide plane is no longer parallel to the laboratory x axis (cf. figure 5). As a result the correlation functions $F_2^{\pi/3}(r_{ij}^*)$ and $F_2^{2\pi/3}(r_{ij}^*)$ with their oscillations between negative and positive values are mixed with $F_2^0(r_{ij}^*)$ (each obtained with the glide plane parallel to the laboratory x axis) and this produces the oscillations in the observed

$F_2^0(r_{ij}^*)$. Above the transition the smectic B phase retains a local herring-bone structure, as we have seen, and it is this which is responsible for the pronounced oscillation in $F_2^0(r_{ij}^*)$ at a scaled temperature of 10.

We now return to the problem of the short range orientational correlations and in particular the maximum observed in the functions $F_4(r_{ij}^*)$ and $F_2^0(r_{ij}^*)$ at a scaled separation of 2 within the smectic E phase. The extent of the orientational correlations is determined by both direct and indirect correlations, the latter being mediated by one or more molecules. In consequence the calculation of the short range correlations is a formidable task and we give here a simple interpretation of our results. Consider the anisotropic function $F_2^0(r_{ij}^*)$ which reflects the orientational correlations for particles located on an axis parallel to the glide plane (cf. figure 1). For a single line of particles interacting via the quadrupolar potential in equation (8) the ground state is a set of particles alternately parallel and orthogonal to the intermolecular vector. The nearest neighbours, corresponding to r_{ij}^* of 1, are therefore anticorrelated and the next nearest neighbours (i.e. $r_{ij}^* = 2$) are correlated. Although this simple observation plays a central role in understanding why the value of $F_2^0(r_{ij}^*)$ is less for r_{ij}^* equal to 1 than for 2 which in turn is greater than for 3, it cannot be the complete explanation. It is clear that molecules in the adjacent, parallel rows, with their indirect contributions to the correlation functions, are essential to stabilize the herring-bone structure and so maintain the molecules along the glide plane more or less parallel.

The majority of experimental investigations of the smectic E and B phases have been concerned with the determination of their molecular organizations using X-ray and neutron diffraction techniques. In this final part of our study we attempt to compare our results with those from such diffraction experiments. The scattering patterns given by our model smectogen could, in principle, be calculated from the orientational correlation functions available from the simulations; however we have adopted an alternative and simpler procedure. In this the X-ray diffraction pattern associated with a particular molecular arrangement is evaluated by first constructing an image or mask of sufficient size that it will diffract a monochromatic beam of light; typically the molecules are scaled to be several mm in magnitude [14].

The optical mask is usually a negative in which the molecules are transparent and the diffraction pattern is recorded photographically with the light beam orthogonal to the mask. The diffraction pattern analogous to that from a crystal plane is obtained by using an optical mask formed from the projection of the molecules onto that plane. The use of an optical transform to determine the appearance of an X-ray diffraction pattern from a given molecular arrangement has the virtue of simplicity, although it does not necessarily possess the accuracy of a numerical Fourier transform of the correlation functions [7].

To construct the diffraction pattern expected for a single smectic layer, with the X-ray beam parallel to the layer normal, we have employed configurations taken from the Monte Carlo simulations to form the optical masks. In these the cross-section of the mesogenic molecule is represented by a line with a length comparable to the lattice spacing (cf. figures 5 and 10). We could have used a more elaborate representation but it is unlikely that this would have affected the optical diffraction pattern significantly. The configurations were taken from the end of the production runs for three scaled temperatures, namely 1, 8 and 17 to simulate the X-ray diffraction patterns from a highly ordered smectic E, a less ordered smectic E and a smectic B phase, respectively. These particular configurations are shown in figure 10; however the masks themselves were circular with a diameter of $24a$. They were constructed by Dr. G. Harburn of

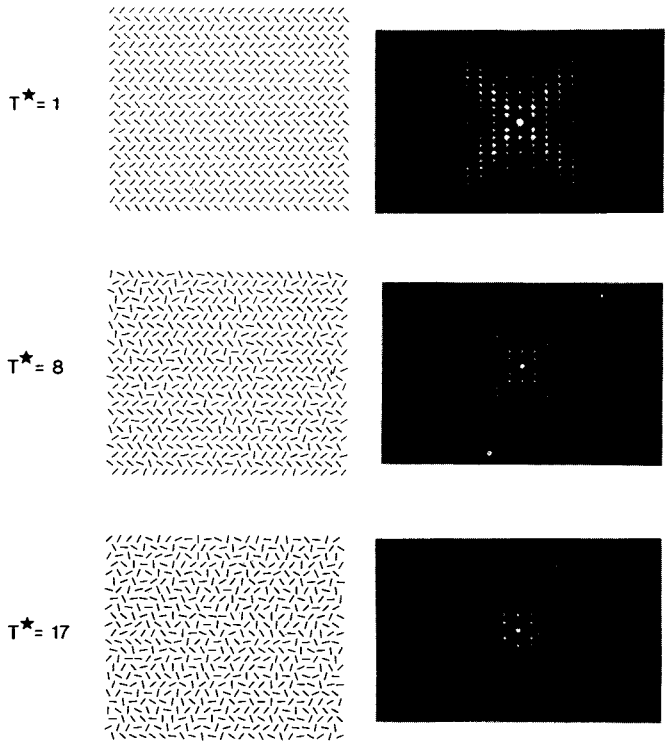

Figure 10. Typical configurations for the smectic E phase ($T^* = 1$ and 8) and for the smectic B phase ($T^* = 17$) together with their optical transforms.

the Department of Physics, University College, Cardiff; he also recorded their optical diffraction patterns and these are given in figure 10 adjacent to the corresponding configuration.

It is instructive, before comparing our simulated patterns with those observed for real smectogens, to consider the form of the diffraction patterns expected for the configurations which we have investigated. We begin with the smectic B phase ($T^* = 17$); because of its rotational disorder the only long range symmetry element is the six-fold rotational symmetry associated with the hexagonal lattice corresponding to the space group $p6$ [31]. Despite this symmetry we have chosen to use the centred rectangular unit cell shown in figure 11 (*a*) because of its natural relationship to that for the smectic E phase, as we shall see. This has now to be used to obtain the so-called reciprocal lattice which is, in essence, the diffraction pattern. To do this we first label the planes, or in our case the lines, of particles which constitute the real lattice using Miller indices, h and k. These give the intercepts of the lines on the crystal axes a and b along the sides of the unit cell as a/h and b/k, where a and b are the dimensions of the unit cell which for the rectangular cell associated with the hexagonal net has a/b equal to $\sqrt{3}$. Examples of such lines, together with their Miller indices, are given in figure 11 (*a*); the distances of the lines from the origin are denoted by d_{hk} and these are also shown. The reciprocal lattice is formed with vectors along d_{hk} whose distance from the origin, d^*_{hk}, is inversely proportional to the length of d_{hk}. This procedure creates an infinite array of points (h k) in reciprocal space; some of the points determined in this way for the hexagonal lattice are shown in figure 11 (*a*). The array

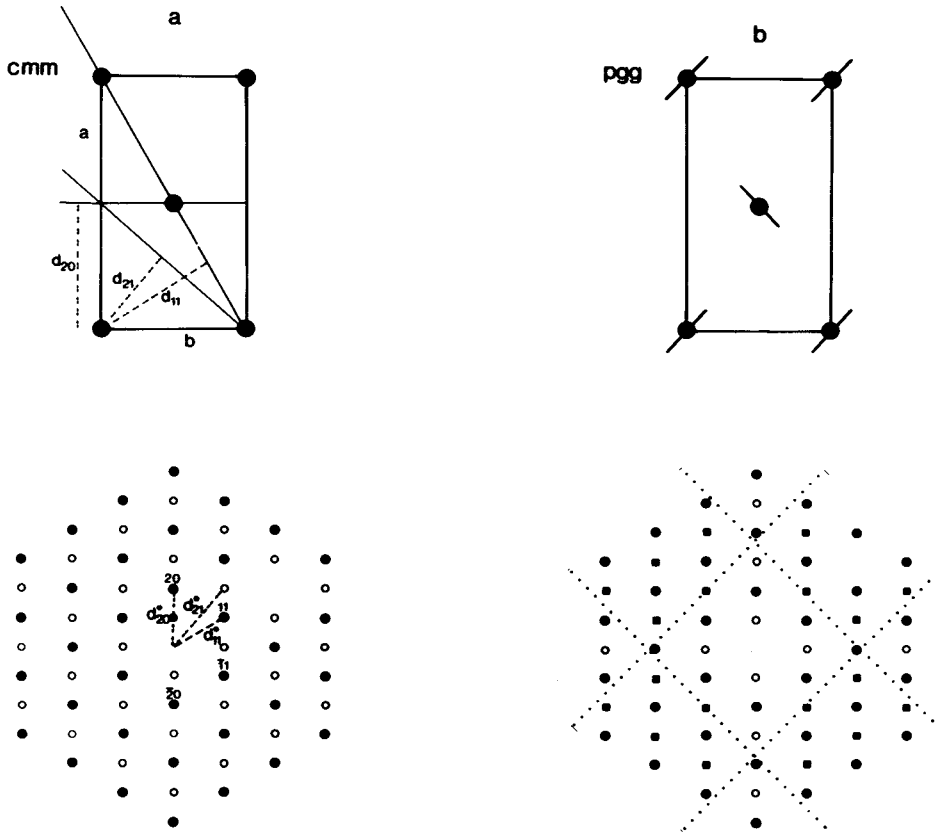

Figure 11. The unit cells, the reciprocal lattices and the axis systems for (*a*) the smectic B and (*b*) the smectic E phases. The open circles denote systematic absences in the reciprocal lattices resulting from the symmetry of the unit cells. The squares indicate those spots which appear in the diffraction pattern of the smectic E but not smectic B phase.

can be compared with the diffraction pattern although the symmetry of the unit cell restricts the points in reciprocal space which contribute to the diffraction pattern. For example, the centred rectangular unit cell for the smectic B phase may be conveniently but not uniquely regarded as belonging to the two-dimensional space group *cmm* and this confines the sum $(h + k)$ to be even [31]; it is these surviving lattice points which are shown in figure 11 (*a*); the open circles denote systematic absences. The central hexagonal arrangement of spots predicted is clearly discernable in the optical diffraction pattern for the smectic B phase (cf. figure 10). Other spots given in the hexagonal arrangement of the reciprocal lattice are also apparent in the optical transform of the simulated configuration but with reduced intensity. However there are twelve diffuse spots just outside the central hexagonal array in the optical diffraction pattern of the smectic B whose presence is not found in the reciprocal lattice for the triangular net; we shall return to these after we have considered the optical transform for the smectic E phase.

The unit cell for a perfectly ordered smectic E phase is also taken to be rectangular (cf. figure 11 (*b*)) but now the herring-bone structure reduces the symmetry. The centring of the unit cell is lost but the two glide planes remain and so the space group

is *pgg* [31]. The points in reciprocal space are obtained in the same way as for the smectic B but the different symmetry of the smectic E requires that for points (h 0) and (0 k), h and k must be even although no other constraints are placed on the Miller indices. These restrictions produce systematic absences along the axes a^* and b^* in reciprocal space corresponding to the glide planes parallel to the axes a and b in real space; the resulting diffraction pattern is shown in figure 11 (*b*), where the location of the absence spots is indicated by open circles. We see that the scattering pattern should contain a hexagonal arrangement of spots with the same positions as those for the smectic B phase. However the pattern differs in the points (h k) for which neither h nor k is zero but their sum is odd; these additional points are shown as squares in figure 11 (*b*). In consequence the reciprocal lattice for the smectic E first varies from that for the smectic B in the presence of four spots labelled (2 1), ($\bar{2}$ 1), ($\bar{2}$ $\bar{1}$) and (2 $\bar{1}$) which sit at the corners of a central rectangle with its major axis along a^* (cf. figure 11 (*b*)). These additional spots are clearly evident in the optical transforms obtained from smectic E configurations for both T^* of 1 and 8, as we can see in figure 10. Additional spots with greater separations, d^*_{hk}, from the origin are also evident in the diffraction pattern of the model smectic E phase but not in that of the model smectic B; we shall not comment further on these because they are of insufficient intensity to be observed in the X-ray scattering patterns of real smectogens. We also note that the sole difference in the diffraction patterns for the smectic E phase at scaled temperatures of 1 and 8 appears to be in the greater scattering intensity for the lower temperature; this is in accord with the higher orientational order at T^* of 1 than 8.

We can now return to the 12 diffuse spots which surround the six sharp spots in the central hexagonal array observed in the optical diffraction pattern from the smectic B configuration ($T^* = 17$). These result from a residual, short range herring-bone structure. As we have seen, the long range herring-bone structure of a smectic E monodomain produces four spots in a rectangular arrangement and these are at the same positions as one-third of the diffuse spots found for the smectic B. The optical transforms of the smectic E phase shown in figure 10 contain a rectangular arrangement of four spots with the major axis along a^* which is orthogonal to the laboratory x axis, defined by reference to the underlying hexagonal lattice of the model (cf. figure 1). When the a axis of the unit cell is rotated by $\pm 60°$ with respect to the x axis to bring the glide plane along the equivalent lattice vectors the diffraction pattern is also rotated by $\pm 60°$. The hexagonal arrangement of spots in reciprocal space are moved to equivalent positions thus leaving the appearance of this part of the scattering pattern unchanged. However those spots for which ($h + k$) is odd but neither h nor k is zero are moved to new positions obtained by rotating the a^* axis through $\pm 60°$ with respect to the x axis. Within the smectic B phase the local glide planes are not arranged along a particular lattice vector but equally along the three equivalent lattice vectors. In consequence the four spots observed for a monodomain become twelve spots for this random arrangement of the glide planes; these spots are diffuse because the herring-bone structure responsible for them is only of short range. Other diffuse spots corresponding to higher orders of reflection but with reduced intensity are also evident in the scattering pattern for the model smectic B phase (cf. figure 10); their origin may also be traced to the local herring-bone structure. It would appear therefore that for our model smectogen the characteristic structure of the smectic E phase persists, at the short range level, far into the smectic B; indeed this is in accord with the pair correlation functions determined by the simulation.

Perhaps the most striking feature of the optical diffraction patterns measured for the smectic E phases ($T^* = 1$ and 8) but not the smectic B is their cross-like form which results from the greater intensity of certain of the spots along orthogonal directions. Their appearance obtains because of the elongated shape of the particles located on the lattice sites. The diffraction pattern is, in fact, a convolution of that from the crystal lattice together with that from the particles located on the lattice sites [32]. So far we have been concerned only with the pattern from the underlying crystal lattice and we must now consider that from the particles forming the model smectogen. These are represented by a line and the scattering pattern from a uniform line of length L and unit scattering power is a band of intensity orthogonal to the molecular line and with a width in reciprocal space of approximately $2/L$ [32]. Strictly the intensity at scattering vector Q along the normal to the band is given by $[2 \sin (LQ/2)/Q]^2$. In our representation of the model mesogen the length of the short axis of a particle is approximately two-thirds of the lattice spacing, which is equivalent to the side of the unit cell b, and so in reciprocal space the intensity should be confined to bands with an approximate width of $3b^*$. For the smectic B phase there is no long range orientational order, the short axes adopt all orientations and so the scattering intensity is uniform in the a^*b^* plane, as we observe for the optical transform at $T^* = 17$. This is not so for the smectic E phase where the particles form two sub-lattices; the particles on each tend to be parallel to one another but the sub-lattices differ in that the preferred directions are mutually orthogonal. In consequence the scattering intensity will be concentrated along two orthogonal bands with widths of approximately $3b^*$. These are marked by the dotted lines in figure 11 (*b*) and are clearly in good agreement with the observed optical diffraction patterns observed for the smectic E phase of the model smectogen (cf. figure 10).

In conclusion we compare the X-ray diffraction patterns measured for real smectogens with these obtained for our model smectogen from the simulation. Such a comparison is not straightforward because the samples studied experimentally are not always pure monodomains; in consequence few orders of reflection are observed and the resolution is often poor. None the less the X-ray diffraction pattern found for the tilted smectic B phase (or smectic H) of terephthalylidene-bis(4-*n*-butylaniline) [7] is in good accord with that measured for the model mesogen. Thus there are six central spots arranged in a regular hexagon together with surrounding regions of diffuse scatter. Indeed these diffuse regions were interpreted as evidence for the local herring-bone structure of the tilted smectic B phase [7]; an interpretation which is confirmed by our simulations. The tilt of the smectic B structure should not influence the scattering pattern in the a^*b^* plane (here c is taken to lie along the molecular long axis); indeed analogous patterns have been observed for the smectic B phase of 4-phenylbenzylidene-4′-amino-*n*-pentyl cinnamate (I) [4, 7]. The experimental X-ray diffraction pattern for the smectic E phase of (I) contains the central, hexagonal arrangement of six spots together with four additional spots forming a central rectangle [4]. Comparable diffraction patterns have been observed from the smectic E and smectic B phases of the iso-butyl analogue of (I) [6]. However the sample of the smectic E contained several domains in which the glide plane was pinned along different lattice vectors; in consequence the scattering pattern contains additional spots obtained by simple rotations of the pattern for a monodomain. These patterns, although of limited extent, are in complete accord with that obtained from the simulation of the smectic E phase which shows many more diffraction spots. Indeed such simulated optical transforms may well be of value in the interpretation of LEED

patterns measured for molecular nitrogen adsorbed on graphite where the resolution is higher [33] than for the X-ray diffraction patterns of smectogens.

We are especially grateful to Dr. G. Harburn (Cardiff) for measuring the optical transforms of the smectic E and B phases as well as for discussions; we also wish to thank Dr. J. M. Seddon (Southampton) for his valuable comments concerning the construction of the reciprocal lattices. Finally we acknowledge the receipt of a Research Studentship from the SERC (PS) and financial support from NATO (GRL and CZ) as well as from CNR and MPI (CZ).

References

[1] FREISER, M. J., 1970, *Phys. Rev. Lett.*, **24**, 1041.
[2] LUCKHURST, G. R., and ROMANO, S., 1980, *Molec. Phys.*, **40**, 129.
[3] See, for example, GOODBY, J. W., and GRAY, G. W., 1984, *Smectic Liquid Crystals* (Leonard Hill).
[4] DOUCET, J., LEVELUT, A. M., LAMBERT, M., LIEBERT, L., and STRZELECKI, L., 1975, *J. Phys., Paris, Coll.*, **36**, C1, 13.
[5] RICHARDSON, R. M., LEADBETTER, A. J., and FROST, J. C., 1978, *Ann. Phys.*, **3**, 177.
[6] LEADBETTER, A. J., FROST, J. C., GAUGHAN, J. P., and MAZID, M. A., 1979 *J. Phys., Paris, Coll.*, **40**, C3, 185.
[7] DOUCET, J., 1979, *The Molecular Physics of Liquid Crystals*, edited by G. R. Luckhurst and G. W. Gray (Academic Press), Chap. 14.
[8] COATES, D., HARRISON, K. J., and GRAY, G. W., 1973, *Molec. Crystals liq. Crystals*, **22**, 99.
[9] MEYER, R. J., 1975, *Phys. Rev.* A, **12**, 1066.
[10] MEYER, R. J., 1976, *Phys. Rev.* A, **13**, 1613.
[11] MICHELSON, A., and CABIB, D., 1977, *Solid St. Commun.*, **23**, 943.
[12] FELSTEINER, J., CABIB, D., and FRIEDMAN, Z., 1978, *Phys. Rev.* A, **18**, 1261.
[13] See, for example, ZANNONI, C., 1979, *The Molecular Physics of Liquid Crystals*, edited by G. R. Luckhurst and G. W. Gray (Academic Press), Chap. 9.
[14] HARBURN, G., TAYLOR, C. A., and WELBERRY, T. R., 1975, *Atlas of Optical Transforms* (Bell).
[15] DIEHL, R. D., TONEY, M. F., and FAIN, S. C., JR., 1982, *Phys. Rev. Lett.*, **48**, 177.
[16] TALBOT, J., TILDESLEY, D. L., and STEELE, W. A., 1984, *Molec. Phys.*, **51**, 1331.
[17] O'SHEA, S. F., and KLEIN, M. L., 1979, *Chem. Phys. Lett.*, **66**, 381.
[18] MOURITSEN, O. G., and BERLINSKY, A. J., 1982, *Phys. Rev. Lett.*, **48**, 181.
[19] EVANS, H., TILDESLEY, D. J., and SLUCKIN, T. J., 1984, *J. Phys.* C, **17**, 4907.
[20] SIMPSON, P., 1983, Ph.D. thesis, University of Southampton.
[21] See, for example, STONE, A. J., 1979, *The Molecular Physics of Liquid Crystals*, edited by G. R. Luckhurst and G. W. Gray (Academic Press), Chap. 2.
[22] METROPOLIS, N., ROSENBLUTH, A. W., ROSENBLUTH, M. N., TELLER, A. H., and TELLER, E., 1953, *J. chem. Phys.*, **21**, 1087.
[23] SAFRAN, S. A., 1981, *Phys. Rev. Lett.*, **46**, 1581. MOURITSEN, O. G., 1983, *Phys. Rev.* B, **28**, 3150.
[24] DENHAM, J. Y., LUCKHURST, G. R., ZANNONI, C., and LEWIS, J. W., 1980, *Molec. Crystals liq. Crystals*, **60**, 185.
[25] HUMPHRIES, R. L., LUCKHURST, G. R., and ROMANO, S., 1981, *Molec. Phys.*, **42**, 1205.
[26] See, for example, ZANNONI, C., 1979, *The Molecular Physics of Liquid Crystals*, edited by G. R. Luckhurst and G. W. Gray (Academic Press), Chap. 3.
[27] LUCKHURST, G. R., ROMANO, S., and SIMPSON, P., 1982, *Chem. Phys.*, **73**, 337.
[28] LUCKHURST, G. R., and SIMPSON, P., 1982, *Molec. Phys.*, **47**, 251.
[29] PRIVMAN, V., and FISHER, M. E., 1983, *J. statist. Phys.*, **33**, 385.
[30] BOWER, D. I., 1981, *J. Polym. Sci.*, **19**, 93.
[31] *International Tables for X-ray Crystallography (1952)*, The International Union of Crystallography (Kinoch Press).
[32] See, for example, LEADBETTER, A. J., 1979, *The Molecular Physics of Liquid Crystals*, edited by G. R. Luckhurst and G. W. Gray (Academic Press), Chap. 13.
[33] DIEHL, R. D., and FAIN, S. C., JR., 1983, *Surf. Sci.*, **125**, 116.